Vortex Identification and Extraction in a Boundary-Layer Flow

Mark Linnick, Ulrich Rist

Institut für Aerodynamik und Gasdynamik
Universität Stuttgart
Pfaffenwaldring 21, 70550 Stuttgart, Germany
Email: rist@iag.uni-stuttgart.de

Abstract

In the present investigation, the scalar quantity λ_2 was used to extract regions ($\lambda_2 < 0$) of concentrated vorticity where the velocity field is mostly of a rotational nature in a particular frame of reference. Further data reduction was achieved by extracting the vortex core lines, serving as a skeletonization of the regions. The extracted vortex regions and core lines are then used as basis for probing the flow, e.g. investigating flow quantities such as vorticity along the core line, and investigating vortex dynamics.

1 Introduction

Steady improvements in measurement techniques and computing power are allowing, respectively, experimentally measured and numerically simulated flow fields to be resolved in space and time with ever increasing accuracy. That one obtains concomitantly an improved description and understanding of complicated flow fields does not necessarily follow, as the fluid physics is more often hidden, than evident, in the large data sets produced. A good example of this is shown in figure 1, which is an instantaneous depiction of fluid vortices in a flat-plate boundary layer undergoing laminar-turbulent transition computed by Meyer [7] using Direct Numerical Simulation (DNS) of the incompressible Navier-Stokes equations. The vortices are visualized as isosurfaces of the scalar λ_2, a quantity which was introduced by [5]. Upstream of $x = 3.2$, the flow is still relatively simple, and three ring-like vortices centered at $z = 0$ are easily recognized upon inspection. Downstream of this location, the flow complexity increases rapidly, placing a large burden on the investigator who must mentally recognize, separate, and group the individual structures in his attempt to understand the flow physics through visualization.

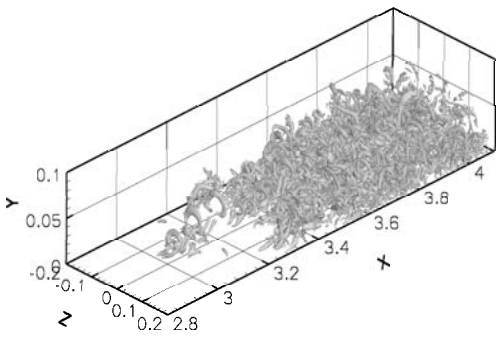

Figure 1: Fluid vortices in the transitional flow over a flat plate visualized using isosurfaces of λ_2. Data from [7].

In the present article, methods are presented that should ease this burden through enhanced visualization that identifies, extracts, and, at a higher abstraction level, analyzes important characteristic features in digital fluid-flow data.

2 Feature Extraction

Features, loosely defined, are the interesting objects of a data set, and are often taken to be regions which satisfy certain constraints, e.g. low pressure, high vorticity magnitude, and so forth. Important features in fluid dynamics include "boundary layers", "high shear-layers" (regions of high shear stress), and 'vortices', for instance. The latter are considered to be important for the role they play in understanding and predicting the behavior of complicated fluid flows, turbulent flows in particular [3].

Despite some controversy with respect to how a 'vortex' should be properly defined for visual-

ization, several plausible methods have evolved recently [5, 8, 13]. Regardless of the method used, once the flow becomes complicated enough, e.g. because turbulent eddies are resolved as in the present DNS data set, the flow field becomes visually cluttered by the sheer amount of interesting features. This is illustrated in figure 1 using the so-called λ_2-method of [5].

To reduce such visual clutter and to make a contribution towards a better understanding of the involved dynamics, researchers have introduced the visualization techniques "feature extraction" and 'tracking' [15, 16, 10], which allows the researcher to concentrate on those features which appear 'interesting' to him, according to some criterion or criteria.

As a first attempt at visually simplifying the flow field shown in figure 1, a seed-growing technique [16] using a simple recursive flood-fill algorithm was implemented. Earlier work applying this technique to separate vortices in transitional flows had been shown to be successful [12]. Using this technique, vortices are separated as follows:

1. Select an isosurface level λ_2^* such that $\lambda_2 \leq \lambda_2^*$ defines the vortex structures. Note that $\lambda_2 < 0$ defines a vortex, and that isosurfaces $\lambda_2 = c_2$ are completely contained inside of isosurfaces $\lambda_2 = c_1$ if $c_2 < c_1$.
2. Select a seed point $\mathbf{x}_s = (x_s, y_s, z_s)$ such that $\lambda_2(\mathbf{x}_s) \leq \lambda_2(\mathbf{x})$ for all $\mathbf{x}$, i.e. find the minimum of λ_2 over the whole field.
3. Starting from the seed point, recursively test neighbors for inclusion. Neighboring points satisfying $\lambda_2 < \lambda_2^*$ are included in the structure.
4. Once all of the points inside the isosurface $\lambda_2 < \lambda_2^*$ containing the seed point found in step 2 have been found, the structure is extracted, and the process can start anew from step 2 to extract the remaining vortices. At this point, of course, the new seed point would not be located inside a vortex that has already been extracted.

In terms of simplification, the seed-growing strategy was found to be less successful in the present case. In figure 2, a sampling of vortices extracted from the data set of figure 1 is presented. Corresponding to this figure, figure 3 depicts the value of λ_2 at a seed point versus the cumulative number of structures found. Upstream of $x = 3.2$, the

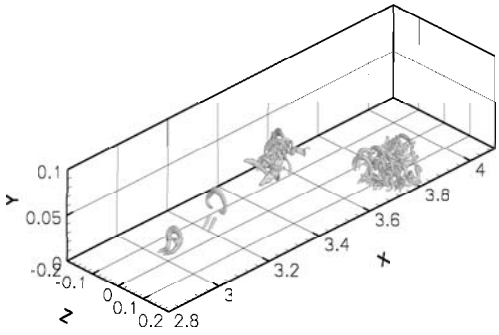

Figure 2: A sampling of vortices extracted from figure 1.

individual vortices are spatially quite distinct, and can be easily extracted using the seed-growing algorithm. Downstream of this location, however, the flow complexity increases rapidly. Vortices tend to merge spatially at the given threshold λ_2^*, with the result that the extraction technique produces a large tangle of twisted vortices. Though the extraction technique considers such a tangle of vortices to be one structure, it is visually clear that several vortices are present. An example of this is seen near $(x, z) = (3.8, 0.1)$ and $(x, z) = (3.6, -0.1)$ in figure 2. As discussed by [16], several additional strategies, such as multidimensional thresholding (i.e. using more than one criterion), are available in cases such as these for further separation. Additionally, one might try a local scaling of λ_2, for example by dividing it by vorticity magnitude. For the present investigation, it was decided that a better approach would be to separate vortices by extracting their core lines (or axes). This strategy is discussed in the following section.

3 Defining Vortex Core Lines

In fluid dynamics textbooks one often makes the approximation that all of the vorticity associated with a vortex is concentrated along a "vortex core line", e.g. [14]. This then leads to the singular distribution of vorticity $\boldsymbol{\omega} = \Gamma\delta(n)\delta(b)\mathbf{s}$ where $\mathbf{s}$ is a unit vector tangent to the vortex core line, n and b are coordinates in the normal and binormal directions, and Γ is the vortex circulation. Intuitively (and implicitly), one selects the vortex core line so that it is located at the geometric center of the vorticity dis-

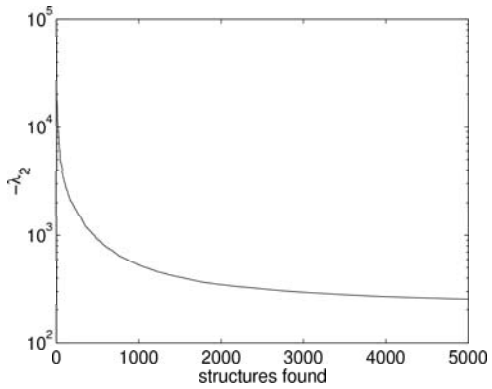

Figure 3: Value of λ_2 at a seed point versus cumulative number of structures found for vortex extraction shown in figure 2. The threshold for the extraction was $\lambda_2^* = -250$, and the total number of found structures was approximately 5500.

tribution in a plane perpendicular to the vortex axis. However, there are other possibilities, as compiled by Roth [13], for instance. One could also use the predictor-corrector technique [1], the "parallel vectors approach" [9] or extremum lines [8] of some scalar quantity to find vortex core lines.

Looking at the data of some classical examples for vortex flows, i.e. the so-called "Rankine Vortex", the "Oseen (or Lamb) Vortex", and the "Burgers Vortex", it is observed that not only vorticity, but also pressure and λ_2 have a local extremum at $r = 0$. As a pressure minimum is in general neither sufficient nor necessary for the existence of a vortex [5], this criterion will not be used to define the vortex core line here. One might consider using local maxima of vorticity with the added constraint that $\lambda_2 < 0$.[1] For the present work we choose to work directly with λ_2 and define core lines as the set of points S in space where λ_2 has a local minimum ("valley lines" of λ_2 in the sense of [8]). The vortex core line is then defined as a one-parameter, three-dimensional space curve $\mathbf{x}(s) = (x(s), y(s), z(s))$ that fulfills the above constraint.

Thus, we are looking for continuous curves in space connecting those points, where, in a plane that contains one point $\mathbf{c} \in S$, and which is perpendicular to the curve's tangent vector, a local minimum of λ_2 occurs at $\mathbf{c}$. This set S is determined as

$$S = \{\mathbf{x} : (\mathbf{H} \cdot \nabla\lambda_2) \times \nabla\lambda_2 = 0 \wedge \eta_2 > 0\} \quad (1)$$

where $\mathbf{H}$ is the Hessian matrix of λ_2, i.e. $(\mathbf{H})_{ij} = \partial^2(\lambda_2)/\partial x_i \partial x_j$, and $\eta_3 \leq \eta_2 \leq \eta_1$ are the eigenvalues of $\mathbf{H}$. Equation (1) indicates that, if $\nabla\lambda_2 \neq \mathbf{0}$ at $\mathbf{c}$, then it is an eigenvector of $\mathbf{H}$.

It should be noted here that we expect to encounter several core lines in a data set like the one shown in figure 1. The according individual core lines connect only subsets of the points in S, but this will be handled by appropriate end and start conditions, as specified further down.

Because we deal with snapshots of an unsteady flow we preferred to use a Galilean invariant vortex criterion over others proposed in the literature, cf. [9, 6]. For us, this aspect is crucial because a non-Galilean invariant method will not be able to detect those vortices which pass by the observer, nor will it show these independent of the local flow speed [5].

3.1 Locating Vortex Cores

In this section, the algorithm selected for determining vortex core lines is described. One possibility investigated was to search for zeros of the quantity $(\mathbf{H} \cdot \nabla\lambda_2) \times \nabla\lambda_2$. But this is critical because of the differentiation involved in computing λ_2 and Eq. (1), despite the fact that we use high-resolution DNS (direct numerical simulation) data and fourth-order central finite differences on a regular grid. So this approach was quickly dismissed, as noise levels, even in filtered numerical data, considerably undermined the resulting accuracy and the following two-pass strategy was used.

A set of points S_a approximating the location of the vortex cores was first obtained. For an arbitrary point $\mathbf{x}_0$, the following strategy was used to test for the existence of a vortex axis in its neighborhood. Using a Taylor series, the scalar field $f(x, y, z) = \lambda_2(x, y, z)$ was expanded about $\mathbf{x}_0$

$$f = f_0 + \mathbf{\Delta x} \cdot \nabla f + \frac{1}{2}\mathbf{\Delta x} \cdot \mathbf{H} \cdot \mathbf{\Delta x} \,. \quad (2)$$

The distance $\mathbf{\Delta x}$ and the gradient ∇f can be rewritten in terms of the eigenvectors $\mathbf{a}_i$ of $\mathbf{H}$

$$\mathbf{\Delta x} = \alpha_1\mathbf{a}_1 + \alpha_2\mathbf{a}_2 + \alpha_3\mathbf{a}_3 \quad (3)$$

$$\nabla f = \beta_1\mathbf{a}_1 + \beta_2\mathbf{a}_2 + \beta_3\mathbf{a}_3 \quad (4)$$

[1] This consideration motivated us to replace pressure by λ_2 in the Banks & Singer predictor-corrector method [18].

so that the Taylor expansion becomes

$$f = f_0 + (\alpha_1\beta_1 + \alpha_2\beta_2 + \alpha_3\beta_3) + \frac{1}{2}(\alpha_1^2\eta_1 + \alpha_2^2\eta_2 + \alpha_3^2\eta_3) \quad (5)$$

or, upon manipulation,

$$f = \tilde{f_0} + \frac{1}{2}\sum_{i=1}^{3}\eta_i(\alpha_i - c_i)^2 \quad (6)$$

where η_i are the eigenvalues of $\mathbf{H}$, $\eta_3 \leq \eta_2 \leq \eta_1$, and $c_i = -\beta_i/\eta_i$. Centering the eigenvector-based coordinate system at point $\mathbf{x}_c = \mathbf{x}_0 + c_1\mathbf{a}_1 + c_2\mathbf{a}_2 + c_3\mathbf{a}_3$, if $\eta_2 > 0$, then f will take on a local minimum in any plane spanned by $\mathbf{a}_2$ and $\mathbf{a}_1$ containing a point on the $\mathbf{a}_3$ axis (see figure 4). A good approximation $\mathbf{x}_a$ for the location of the vortex axis, then, is $\mathbf{x}_a = \mathbf{x}_0 + c_1\mathbf{a}_1 + c_2\mathbf{a}_2$, if the corresponding $|\mathbf{\Delta x}|$ is not too large to render the Taylor series approximation inaccurate. We note that a similar strategy for locating vortex core lines was used by [8] in their sectionally minimal pressure method, where they take $f(x, y, z) = p(x, y, z)$, the fluid pressure.

Using the above method, the set S_a is determined by visiting every grid-point $\mathbf{x}_0$ in the discrete numerical data, and if $\lambda_2 < 0$ at this point

1. finding the approximate distance $\mathbf{\Delta x} = c_1\mathbf{a}_1 + c_2\mathbf{a}_2$ to the nearest vortex core line located at $\mathbf{x}_a = \mathbf{x}_0 + \mathbf{\Delta x}$, and
2. if $|\mathbf{\Delta x}| < h$, where h is a measure of the local grid step-size (grids were not necessarily equidistant), adding the point $\mathbf{x}_a$ to the set S_a.

Next, the points in the set S_a are refined by doing a local minimization of λ_2 in planes spanned by eigenvectors $\mathbf{a}_1$ and $\mathbf{a}_2$ of its Hessian. Starting at the point $\mathbf{x}^i = \mathbf{x}_a \in S_a$, the algorithm iteratively

1. computes the eigenvectors $\mathbf{a}_1$ and $\mathbf{a}_2$ of the Hessian of λ_2 at $\mathbf{x}^i$, and
2. minimizes λ_2 in the plane spanned by $\mathbf{a}_1$ and $\mathbf{a}_2$ to determine guess $\mathbf{x}^{i+1}$,

until convergence, defined as the iteration i at which $\mathbf{x}^i$ no longer changes significantly. The minimization was accomplished using the NEWUOA unconstrained minimization software from [11].

Once the set of points lying on the vortex axes has been determined, they are linked together to trace out the vortex axis. For this purpose, a line-linking algorithm similar to that described in [17] has been implemented. Starting from a given point $\mathbf{x}_0$ in S, a search is performed for the next closest point in S which minimizes the function $g = |\mathbf{\Delta x}|/h + 2\theta/\pi$, where θ is the angle between eigenvector $\mathbf{a}_3$ at this point and point $\mathbf{x}_0$, $|\mathbf{\Delta x}|$ is the distance between the two points, and h is a measure of the local grid step-size.

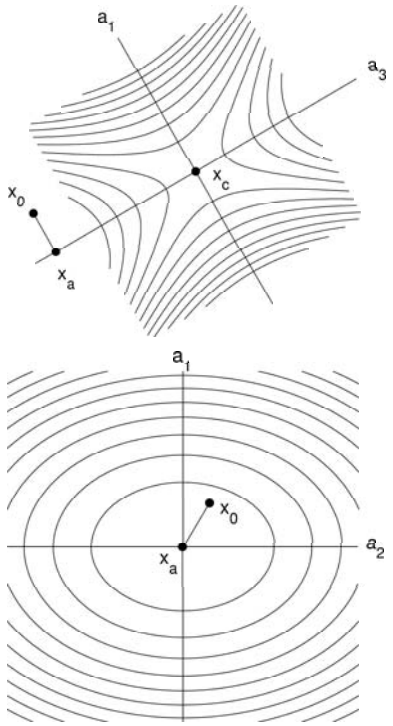

Figure 4: Finding the approximate location $\mathbf{x}_a$ of a vortex axis: contours of the approximation given in Eq. (6) with $\eta_3 < 0$.

Verifications of the algorithm have been performed with cartesian three-dimensional scalar fields that contained a straight tubular structure or a torus-like 'vortex', both oriented at an arbitrary angle with respect to the grid. The results (not shown here) indicated that the method was able to correctly locate the "vortex axis" of these structures. An evaluation of the errors and a grid refinement study revealed that the error decreases according to the second-order central finite-difference discretization used for spatial derivatives.

4 Results

4.1 Vortex Core Line Extraction

The vortex core extraction algorithm described above was applied to the data set shown in figure 1. Only part of the domain, $x = [3.2, 3.5]$, is considered so that more detail can be seen in the resulting figures. Figure 5 depicts the vortex structures using isosurfaces of λ_2. Core lines extracted from these structures are shown in figure 6. By reducing the vortices to their core lines, the amount of data required to represent the vortices has been drastically reduced. In figure 7, these core lines have been thickened for improved visualization by giving them a constant, finite radius. Although this has not yet been investigated, one could consider basing the radius on a physically meaningful quantity such as that which yields a constant vortex circulation $\Gamma = \oint \mathbf{u} \cdot d\mathbf{x}$ in a plane perpendicular to the vortex axis.

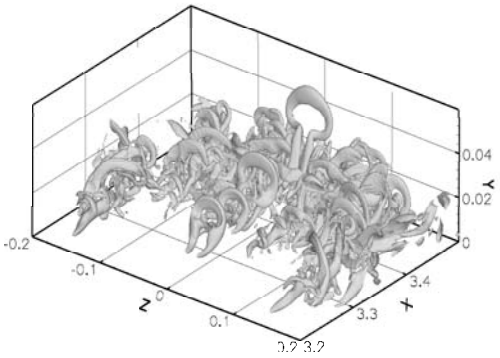

Figure 5: Zoom-in of the region $x = [3.2, 3.5]$ in figure 1.

Unlike the seed-growing strategy discussed earlier, core line extraction allows individual vortices to be easily separated. An example is shown in figure 8. Here, random vortices from figure 7 have been selected and highlighted so that they are now more easily distinguished, in contrast to their neighbors. Of course, the random part of the selection process could be replaced by physically-based criteria specified by the user. The strongest, largest, or otherwise "most interesting" vortices are then highlighted as shown, and tracked in time so that the investigator can observe their time-dependent behavior.

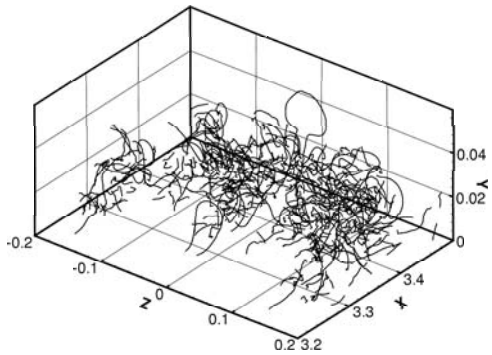

Figure 6: Extracted core lines of vortices shown in figure 5.

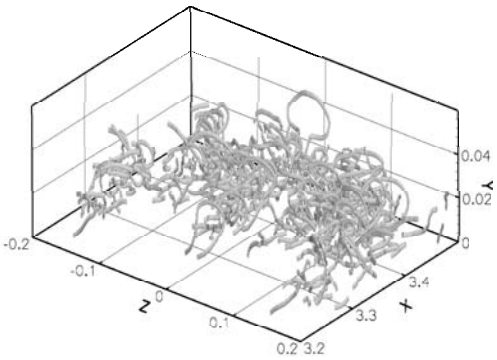

Figure 7: Vortices reconstructed from core lines shown in figure 6.

Figure 9 depicts selected core lines from figure 8 along with eigenvector $\mathbf{a}_3$ along the core line. As far as this is possible to visually confirm in the graphical representation, the eigenvector $\mathbf{a}_3$ appears to be tangent to the extracted core line, indicating that approximately the same core line would have been extracted had a space-marching procedure been used to extract the core line. In such a scheme, one finds a point on the core line, then steps in space a small distance $\Delta\mathbf{x}$ in the direction of $\mathbf{a}_3$ at the found point. This new point is used as guess for finding the next point on the core line as the minimum of λ_2 in a plane spanned by $\mathbf{a}_1$ and $\mathbf{a}_2$. Thus

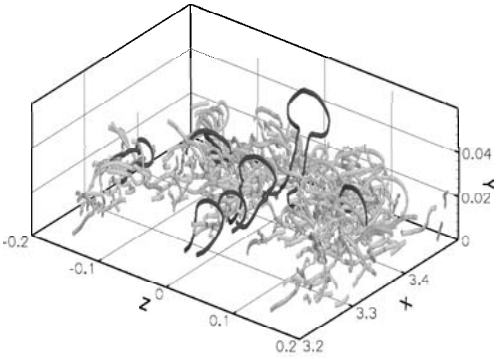

Figure 8: Arbitrarily chosen vortices from figure 7 emphasized.

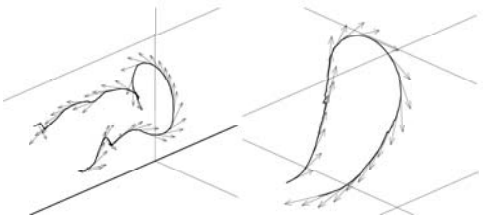

Figure 9: Selected core lines from figure 6 along with eigenvector $\mathbf{a}_3$ of $\mathbf{H}(\lambda_2)$ at selected points along the core line.

our method is comparable to Banks & Singer [1] with the exception that it uses only λ_2 data.

In figure 10, several vortex core lines (denoted by the symbol •) have been selected, and one point on each core line taken as a starting point for integrating the vorticity field $\boldsymbol{\omega}$ to compute *vortex lines*. Vortex lines (not to be confused with vortex *core* lines) have the property that they are everywhere tangent to the vorticity vector $\boldsymbol{\omega} = (\omega_x, \omega_y, \omega_z)$. They are the solution families of the differential equations [14]

$$\frac{dx}{\omega_x} = \frac{dy}{\omega_y} = \frac{dz}{\omega_z} \tag{7}$$

The accuracy of the streamtrace integration was checked by decreasing the integration step-size, and confirming that the same vortex line was obtained. The computed vortex lines appear to correspond fairly well with the extracted vortex core lines which indicates that minimum lines of λ_2 are physically meaningful to trace vortex cores. Note that using vortex lines is not appropriate in a boundary layer (i.e. close to a wall) because vorticity doesn't distinguish between shear layers and vortices. This is why the vortex lines in Fig. 10 extend beyond the vortices and follow the shear layer at the wall in Z-direction for small Y.

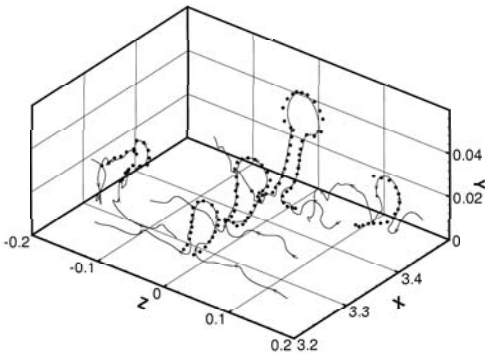

Figure 10: Vortex lines computed by integrating the vorticity field $\boldsymbol{\omega}$ forwards and backwards starting from a point on the vortex core lines. Location of the vortex core lines indicated with the symbol •.

4.2 Higher Level Analysis: Vortex Dynamics

In [3], the statement is made that "vortex dynamics is the missing mathematical framework for the study of coherent structures". Through vortex dynamics, the evolution and interaction of the coherent structures is directly connected to their topology and strength.

The most important mathematical equations governing vortex dynamics are

$$\mathbf{u}(\mathbf{x}, t) = \frac{1}{4\pi} \int \frac{\boldsymbol{\omega}(\mathbf{x}', t) \times (\mathbf{x} - \mathbf{x}')}{|\mathbf{x} - \mathbf{x}'|^3} \, d\mathbf{x}' \tag{8}$$

which, in the absence of boundaries, determines the velocity field $\mathbf{u}$ for a given vorticity field $\boldsymbol{\omega}$, and

$$\frac{D\boldsymbol{\omega}}{Dt} = \boldsymbol{\omega} \cdot \nabla \mathbf{u} + \nu \nabla^2 \boldsymbol{\omega} \tag{9}$$

which determines the temporal evolution of the vorticity field. In this equation, $D(\cdot)/Dt = \partial(\cdot)/\partial t +$

$\mathbf{u} \cdot \nabla(\cdot)$, and ν is the kinematic viscosity of the fluid. The first equation is often called the Biot-Savart law, while the second is known as the vorticity transport equation.

Using the Biot-Savart law, one can consider investigating the interaction of individual vortex structures by first separating them using feature extraction. The contribution to the induced velocity field from any given vortex is then *defined* as the velocity that results from substituting into equation (8) only the vorticity $\boldsymbol{\omega}$ contained within the vortex itself; outside of the vortex $\boldsymbol{\omega} \equiv 0$ in this integral. A sample visualization is shown in figure 11. Here, the vortex has been separated using the region-growing technique. Using the vorticity inside the isosurface $\lambda_2 < \lambda_2^*$, the Biot-Savart law is numerically integrated over the whole domain to compute the induced velocity field shown. The singularity in the integral has been handled by a simple cut-off procedure for $|\mathbf{x} - \mathbf{x}'| < \varepsilon$, and the numerical integration itself was computed using standard midpoint-rule quadrature. More accurate and efficient methods for computing this integral include the multipole methods discussed in references [2, 4, 19].

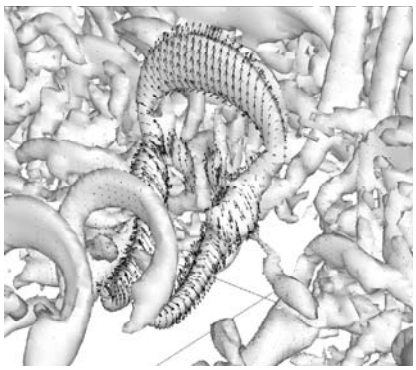

Figure 11: Velocity induced via equation (8) by the vorticity inside a selected vortex.

The induced velocity shown in figure 11 appears as expected: the flow rotates about the vortex core line in a sense determined by the locally aligned vorticity field. This should be compared with the relative velocity on the surface of the vortex shown in figure 12. The vortex surfaces shown here were reconstructed from the vortex core lines as was done for figure 7, and the relative velocity was obtained

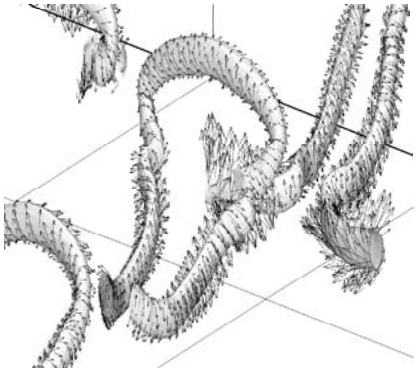

Figure 12: Velocity on vortex surface relative to velocity at vortex core.

by selecting a point on the vortex core line (1), determining the intersection of a plane perpendicular to the vortex core line with the vortex surface (2), and at selected points along the curve forming this intersection, subtracting from the velocity at these points the velocity at the point (1) on the vortex core line. This process was repeated for a regular distribution of points along the vortex core line.

It appears that both techniques present a viable way to convey the sense of rotation of individual vortices to the observer. Further work is necessary to assess possible quantitative differences between the two. In addition it will be very interesting to try to identify the mutual interactions between different vortices using the Biot-Savart law.

5 Conclusions and Future Work

Based on the scalar quantity λ_2 vortices have been identified, visualized, and separated. An algorithm that traces the spatial minima of λ_2 successfully extracted vortex core lines. Possibly for the first time it was shown that minimum lines of λ_2 are physically meaningful to trace vortex cores. The skeletonization of vortices was then very helpful to segment the data, i.e. to separate individual vortices which would appear connected if a single λ_2 threshold were used. The core lines form an ideal basis for probing the flow, e.g. investigating flow quantities such as vorticity or others along the core line, or for investigating vortex dynamics, as shown in the examples. Tracking of the observed structures with respect to time and comparing their evolution with

the predictions using the Biot-Savart law are needed in order to understand whether the vortex dynamics can be fully captured based on instantaneous data.

It was also found that the vorticity ω_p possesses a local extremum at a point on the vortex core line and in a plane perpendicular to eigenvector $\mathbf{a}_3$. Another vortex core line extraction method making use of both λ_2 and $\boldsymbol{\omega}$ was therefore successfully implemented and tested in [18]. As pointed out by [13], these, and other possible methods define line-type features by minimizing a scalar quantity s in a vector field $\mathbf{v}$ by finding the set of points where $\nabla s \parallel \mathbf{v}$. In the present case, $s = \lambda_2$ and $\mathbf{v} = \mathbf{a}_3$.

As mentioned earlier, vortices are only one amongst other coherent structures of importance in fluid dynamics. Our next step will be to evaluate methods for shear layer visualization. As in the case of vortex detection, using vorticity alone to detect high shear layers would be ambiguous.

References

[1] D. C. Banks and B. A. Singer. Vortex tubes in turbulent flows: Identification, representation, reconstruction. In R. D. Bergeron and A. E. Kaufman, editors, *Proceedings of IEEE Visualization*, pages 132–139, October 1994.

[2] R. K. Beatson and L. Greengard. A short course on fast multipole methods. In M. Ainsworth, J. Levesley, W. Light, and M. Marletta, editors, *Wavelets, Multilevel Methods and Elliptic PDEs*, pages 1–37. Oxford University Press, 1997.

[3] J. Bridges, H. Husain, and F. Hussain. Whither coherent structures? comment 1. In J. L. Lumley, editor, *Whither Turbulence? Turbulence at the Crossroads.*, volume 357 of *Lecture Notes in Physics.*, pages 132–151. Springer-Verlag, New York, 1990.

[4] G.-H. Cottet and P. D. Koumoutsakos. *Vortex Methods: Theory and Practice*. Cambridge University Press, 2000.

[5] J. Jeong and F. Hussain. On the identification of a vortex. *J. Fluid Mech.*, 285:69–94, 1995.

[6] M. Jiang, R. Machiraju, and D. Thompson. Detection and visualization of vortices. In *Visualization Handbook*. Academic Press, 2003. unpublished.

[7] D. Meyer. *Direkte numerische Simulation nichtlinearer Transitionsmechanismen in der Strömungsgrenzschicht einer ebenen Platte.* PhD thesis, Universität Stuttgart, 2003.

[8] H. Miura and S. Kida. Identification of tubular vortices in turbulence. *J. Phys. Society Japan*, 66(5):1331–1334, 1996.

[9] R. Peikert and M. Roth. The parallel vectors operator - a vector field visualization primitive. In D. S. Ebert, M. Gross, and B. Hamann, editors, *Proceedings of IEEE Visualization*, pages 263–270. IEEE Computer Society Press, October 1999.

[10] F. H. Post, B. Vrolijk, H. Hauser, R. S. Laramee, and H. Doleisch. The state of the art in flow visualization: Feature extraction and tracking. *Computer Graphics Forum*, 22(4):775–792, 2003.

[11] M. J. D. Powell. On the use of quadratic models in unconstrained minimization without derivatives. DAMTP Numerical Analysis Group Report 2003/NA03, Cambridge University, 2003.

[12] U. Rist, K. Müller, and S. Wagner. Visualization of late-stage transitional structures in numerical data using vortex identification and feature extraction. In *8th International Symposium on Flow Visualization*, 1998. Paper no. 103.

[13] M. Roth. *Automatic Extraction of Vortex Core Lines and Other Line-Type Features for Scientific Visualization*. PhD thesis, ETH Zürich, 2000.

[14] P. G. Saffman. *Vortex Dynamics*. Cambridge University Press, 1992.

[15] R. Samtaney, D. Silver, N. Zabusky, and J. Cao. Visualizing features and tracking their evolution. *IEEE Computer Visualization*, 27(7):20–27, 1994.

[16] D. Silver. Object-oriented visualization. *IEEE Computer Graphics and Application*, 15(3):20–27, 1995.

[17] C. Steger. An unbiased detector of curvilinear structures. Technical Report FGBV-96-03, Technische Universität München, 1996.

[18] S. Stegmaier, U. Rist, and T. Ertl. Opening the can of worms: An exploration tool for vortical flows. In *Proceedings of IEEE Visualization*, 2005.

[19] J. Strain. Locally corrected multidimensional quadrature rules for singular functions. *SIAM J. Sci. Comput.*, 16(4):992–1017, 1995.